cmgh
CELLULAR AND MOLECULAR GASTROENTEROLOGY AND HEPATOLOGY

ORIGINAL RESEARCH

Nonalcoholic Steatohepatitis Disrupts Diurnal Liver Transcriptome Rhythms in Mice

Leonardo Vinicius Monteiro de Assis,[1] Münevver Demir,[2,3] and Henrik Oster[1]

[1]Institute of Neurobiology, Center of Brain Behavior and Metabolism, University of Lübeck, Lübeck, Germany; [2]Department of Hepatology and Gastroenterology, Charité-Universitätsmedizin Berlin, Campus Virchow-Klinikum, Berlin, Germany; and [3]Department of Hepatology and Gastroenterology, Charité-Universitätsmedizin Berlin, Campus Charité Mitte, Berlin, Germany

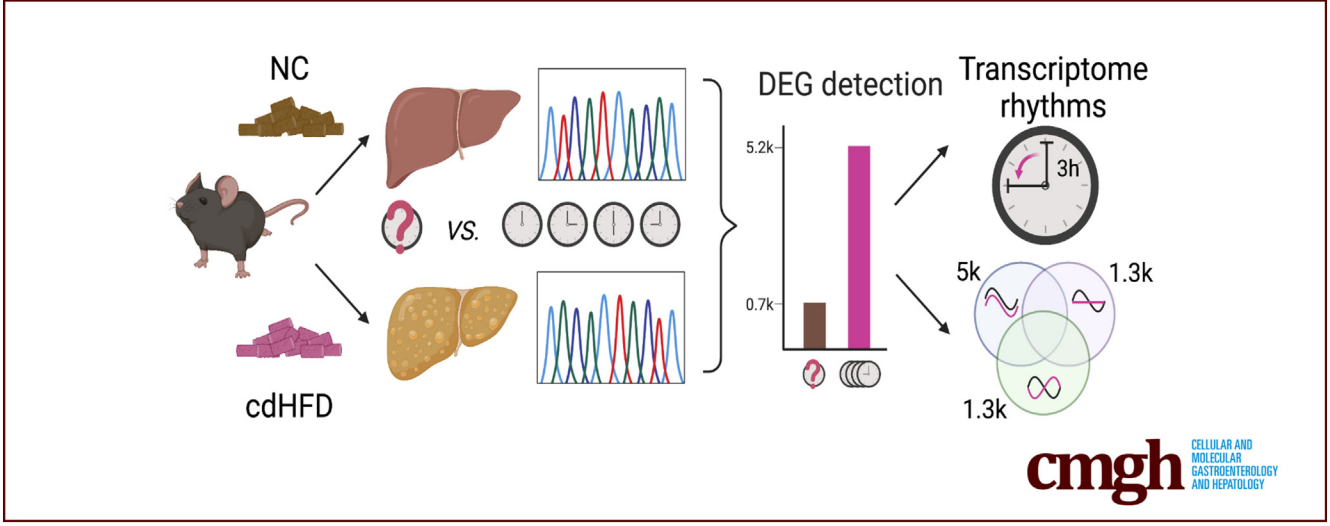

SUMMARY

Circadian profiling improves target gene detection and pathway characterization in mouse models of nonalcoholic steatohepatitis. Fatty livers show 3-hour advances in metabolic and clock gene transcript rhythms. Circadian profiling further reveals temporal changes in lipid, carbohydrate, and cholesterol metabolic transcripts.

BACKGROUND & AIMS: The liver ensures organismal homeostasis through modulation of physiological functions over the course of the day. How liver diseases such as nonalcoholic steatohepatitis (NASH) affect daily transcriptome rhythms in the liver remains elusive.

METHODS: To start closing this gap, we evaluated the impact of NASH on the diurnal regulation of the liver transcriptome in mice. In addition, we investigated how stringent consideration of circadian rhythmicity affects the outcomes of NASH transcriptome analyses.

RESULTS: Comparative rhythm analysis of the liver transcriptome from diet-induced NASH and control mice showed an almost 3-hour phase advance in global gene expression rhythms. Rhythmically expressed genes associated with DNA repair and cell-cycle regulation showed increased overall expression and circadian amplitude. In contrast, lipid and glucose metabolism–associated genes showed loss of circadian amplitude, reduced overall expression, and phase advances in NASH livers. Comparison of NASH-induced liver transcriptome responses between published studies showed little overlap (12%) in differentially expressed genes (DEGs). However, by controlling for sampling time and using circadian analytical tools, a 7-fold increase in DEG detection was achieved compared with methods without time control.

CONCLUSIONS: NASH had a strong effect on circadian liver transcriptome rhythms with phase- and amplitude-specific effects for key metabolic and cell repair pathways, respectively. Accounting for circadian rhythms in NASH transcriptome studies markedly improves DEG detection and enhances reproducibility. *(Cell Mol Gastroenterol Hepatol 2023;16:341–354; https://doi.org/10.1016/j.jcmgh.2023.05.008)*

Keywords: Circadian RNAseq; Nonalcoholic Fatty Liver Disease (NAFLD); Circadian Clock; Energy Metabolism; Circadian Bioinformatics.

See editorial on page 497.

Living beings are subject to rhythmic changes in environmental factors such as light and temperature. Mammals use internal circadian clocks to anticipate such regular changes and adjust physiological processes to meet environmental demands.[1,2] Most biological processes show rhythmic activity such as heart rate, DNA repair,

energy metabolism, and immunity.[1,3–5] At the cellular level, circadian timekeeping is based on interlocked transcriptional-translational feedback loops of clock genes and proteins. The clock transcriptional-translational feedback loop orchestrates physiological rhythms through transcriptional programs of clock-controlled genes.[3]

Circadian clocks are present in most cells and tissues, including liver. Although the importance of circadian rhythms in liver physiology is well known, many basic and clinical studies often pay little attention to this factor when taking and analyzing samples. A recent study evaluated the top-50 cited reports in 10 different fields between 2015 and 2019, showing that only 6.1% of the studies included time-of-day information.[6] In recent years, the advances in omics techniques and analysis have clearly shown that a substantial portion of the transcriptome, proteome, and metabolome shows rhythmic patterns.[7–11] Therefore, a lack of temporal control may severely affect study outcome and reproducibility.

The prevalence of nonalcoholic fatty liver disease (NAFLD) is estimated at 25%–30% worldwide.[12] NAFLD may progress to liver inflammation with tissue damage, a phenotype known as nonalcoholic steatohepatitis (NASH). If not treated, NASH can progress to cirrhosis or hepatocellular carcinoma. Unfortunately, no specific drug treatment for NAFLD is yet approved.[13,14] NASH results from an imbalance of lipid metabolic processes such as lipogenesis, β-oxidation, and secretion of triglycerides from the liver, as well as endoplasmic reticulum stress, inflammation, and insulin resistance, most of which are under circadian control.[3,13,15–18] Disruption of circadian rhythms has been shown to hasten NASH and hepatocellular carcinoma in mice.[19]

Several studies have identified gene signatures of NASH in mice and human beings to develop prognostic markers.[20,21] Considering that a large portion of the liver transcriptome is rhythmic, we hypothesized that diurnal profiling of gene expression would critically improve detection of differentially expressed genes (DEGs) in this context.

Results

Time Stamping of Tissue Sampling Improves Detection of DEGs in NASH

Our initial step was to evaluate how consistent DEGs were identified between different studies using similar NASH mouse models. Three independent studies using high-fat diet containing high fructose and cholesterol (HFFC)-induced NASH in C57BL/6J mice were chosen.[22–24] RNA sequencing (RNAseq) data were reanalyzed with identical parameters in DESeq2.[25] A total of 5608 NASH-dependent DEGs were identified across all 3 studies, but only 688 (12%) NASH shared DEGs were identified at the same time in all 3 data sets (Figure 1*A*, Supplementary Table 1). Considering the marked rhythmicity of the liver transcriptome and liver metabolism,[11,26] one explanation for this lack of consistency would be differences in sampling times and control thereof between studies.

We compared identified DEGs against the Circa database of circadian gene expression,[11] and, indeed, 52% of the 5608 DEGs detected across studies and 58% of the shared 688 DEGs were rhythmic (Figure 1*B* and *C*, Supplementary Table 1). Three principal scenarios are possible in which rhythmicity of gene expression may influence results in a non–time-controlled test scenario (Figure 1*D*): if a gene is stably (ie, without rhythm) expressed under both conditions (Figure 1*D*, left panel), then tissue sampling time will have no effect on the outcome of the comparison. However, once DEG expression is rhythmic in any of the 2 conditions, alterations in mesor (baseline expression), amplitude (variation across time), and acrophase (time of peak expression) may lead to different results depending on the time of sampling (Figure 1*D*, right panels). This prompted us to study NASH-induced changes in liver gene expression by profiling transcriptome regulation across 24 hours.

Effects of NASH on the Diurnal Regulation of the Liver Transcriptome

Mice of both sexes were kept on choline-deficient high-fat diet (cdHFD) for 2 weeks for rapid NASH induction,[27] which was marked by increased lipid and cholesterol accumulation, marked histologic alteration, and increased serum marker for liver damage (aspartate aminotransferase) (Figure 2) as corroborating a previous study.[28] Liver samples from cdHFD and normal chow (NC) control animals were collected at 6-hour intervals over 24 hours and subjected to RNAseq (Figure 3*A*). Initially, comparable with previous studies, we evaluated DEGs irrespective of sampling time by pooling data for each condition. This approach yielded 1684 DEGs (1214 up-regulated and 470 down-regulated) (Supplementary Table 2). When DEG analysis was performed for each time point (*zeitgeber* time, ZT) separately, 1664 time-dependent DEGs (tdDEGs) were detected, 80% of which overlapped with the DEGs detected in the previous studies (Figure 3*B*, Supplementary Table 2). Among the tdDEGs, 337 genes were consistently up-regulated or down-regulated at every single time point in NASH (Figure 3*C*). Comparison of these robust DEGs with DEGs from previous studies (Figure 1) showed a high overlap of 93% (314 genes). There were 181 robust DEGs detected in all data sets (Supplementary Table 2), constituting a set of bona fide transcriptional NASH markers. Gene set enrichment analysis (GSEA) of robust DEGs showed several NASH-relevant biological processes such as sterol, lipid, and cholesterol metabolism, inflammation, and insulin signaling[29] (Figure 3*D* and examples in *E*, Supplementary Table 2).

Abbreviations used in this paper: **cdHFD, choline-deficient and methionine-low high-fat diet; Chipseq, Chromatin immunoprecipitation sequencing; DBP, D-box binding PAR BZIP transcription factor; DEG, differentially expressed gene; DRG, differentially rhythmic gene; GSEA, gene set enrichment analysis; HFD, high-fat diet; HFFC, high-fat diet containing high fructose and cholesterol; JTK, Jonckheere-Terpstra-Kendall; LD, light/dark conditions; NAFLD, nonalcoholic fatty liver disease; NASH, nonalcoholic steatohepatitis; NC, normal chow; RNAseq, RNA sequencing; tdDEG, time-dependent differentially expressed gene; ZT, *zeitgeber* time.**

Most current article

© 2023 The Authors. Published by Elsevier Inc. on behalf of the AGA Institute. This is an open access article under the CC BY-NC-ND license (http://creativecommons.org/licenses/by-nc-nd/4.0/).

2352-345X
https://doi.org/10.1016/j.jcmgh.2023.05.008

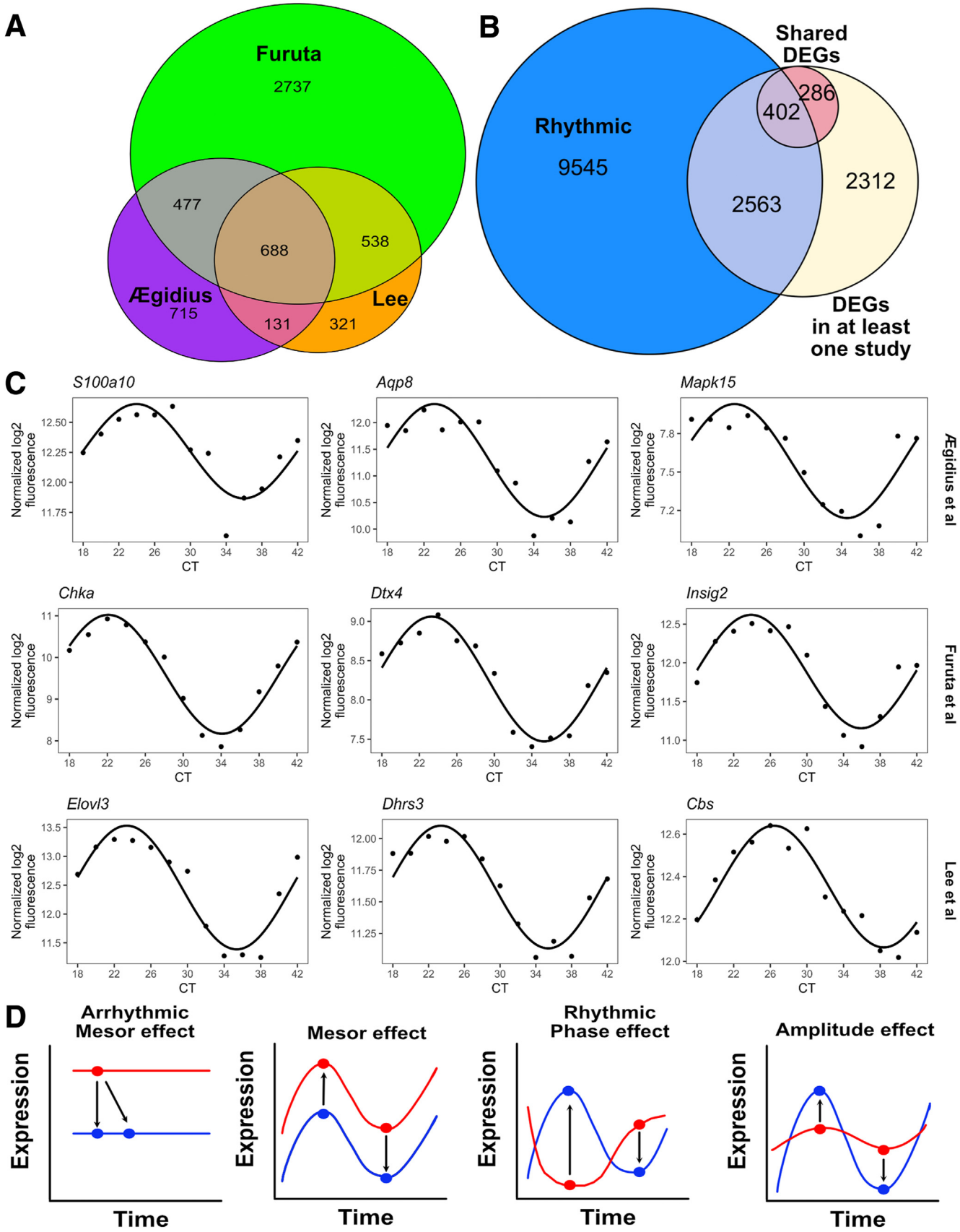
A
Furuta
2737
Ægidius
715
Lee
477
688
538
131
321
B
Rhythmic
9545
Shared
DEGs
286
402
2563
2312
DEGs
in at least
one study
C
S100a10
Aqp8
Mapk15
Chka
Dtx4
Insig2
Elovl3
Dhrs3
Cbs
Normalized log2
fluorescence
CT
Ægidius et al
Furuta et al
Lee et al
D
Arrhythmic
Mesor effect
Mesor effect
Rhythmic
Phase effect
Amplitude effect
Expression
Time

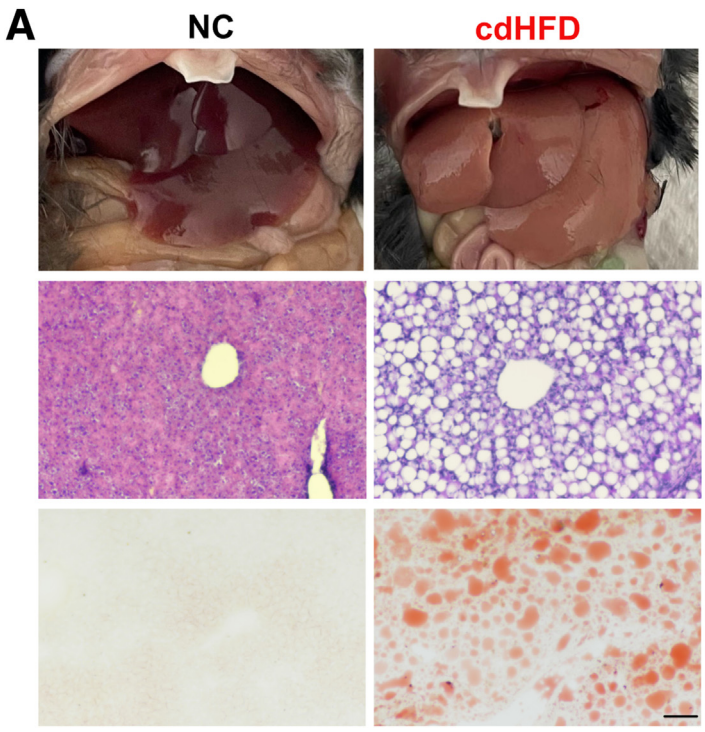

Figure 2. cdHFD leads to extensive liver steatosis and tissue damage. (*A*) Representative macroscopic evaluation of the liver (*upper row*), H&E staining (*middle row*), and Oil Red O (ORO) staining (*lower row*) of NC and cdHFD mice. *Scale bar*: 100 μm for all micrographs. (*B*) Serum aspartate aminotransferase (AST; n = 5 per group) and tissue cholesterol (n = 20 per group) levels. $^{**}P < .01$ by unpaired Student *t* test.

NASH Phase-Advance Liver Transcriptome Rhythms

A total of 5151 and 4215 genes showed significant circadian rhythmicity in either control or NASH livers, respectively, but only 1714 of these retained rhythmicity across both conditions (Figure 4*A*, Supplementary Table 3). Only slight differences in acrophase distribution between groups were found, with the highest number of genes peaking around the night–day transition (ZT23) (Figure 4*B*). Remarkably, a marked phase advance of approximately 3 hours on average was observed in the rhythms of robustly rhythmic genes in NASH (Figure 4*C*). This phase advance was mirrored in a marked shift in circadian clock gene expression rhythms (Figure 4*D*). To distinguish between NASH and high-fat diet (HFD) effects, we compared cdHFD data with a previously published HFD data set.[10] On average, core clock gene rhythms were reduced for mesor, phase, and amplitude under cdHFD conditions, and these effects were not observed (mesor, amplitude) or were expressed much less on a HFD, suggesting NASH-specific responses (Figure 4*E* and *F*, Supplementary Table 3). A definition and a flowchart of all categories of DEGs are provided (Figure 4*G*).

The comparable NASH-induced phase advance in the expression profiles of core clock and rhythmic genes suggested a liver clock–mediated process. To further evaluate this, we extracted direct targets of core clock transcription factors (Basic helix-loop-helix ARNT like 1, BMAL1, Nuclear receptor subfamily 1 group D member 1, Nuclear receptor subfamily 1 group D member 1, NR1D1, Circadian locomoter output cycles protein kaput, CLOCK, and D-box binding PAR BZIP transcription factor, DBP/Adenovirus E4 promoter binding protein 4,E4BP4) using the Chromatin Immunoprecipitation Sequencing (Chipseq) Atlas database.[30] We identified 294, 1067, 70, and 358 bona fide targets of BMAL1, NR1D1, CLOCK, and DBP/EBP4, respectively, which also were rhythmic in at least 1 diet condition and showed alterations in mesor, amplitude, or phase (Supplementary Table 4). Across all of these clock transcription factor targets, reductions in mesor and amplitude as well as robust phase advances were observed (Figure 5*A*). Exclusive targets were filtered and selected for each clock transcription factor and analyzed for phase responses. Supporting our assumption, a marked phase advance (of 4 hours on average) was observed (Figure 5*B–D*, Supplementary Table 4). Together, these data suggest that NASH induction phase advances the liver clock and, subsequently, clock-controlled genes.

NASH Induced Damping and Phase Advance of Lipid Metabolic Pathways

To assess the metabolic effects of transcriptome rhythm alterations in NASH, we quantitatively evaluated changes in

Figure 1. (***See previous page***). **DEGs from similar NASH studies show a remarkably small concordance.** (*A*) Venn diagram represents the DEGs of 3 independent studies analyzed using DESeq2 (adjusted *P* value $< .01$ and fold change $> \pm 1$). (*B*) Venn diagram shows the number of DEGs (identified in panel *A*) that are rhythmic according to liver circadian transcriptome collected every 2 hours over a 48-hour period. Shared DEGs (688) were identified by evaluating 3 independent studies. (*C*) Representative circadian profiles of exclusively detected DEGs in each data set. (*D*) *Blue curves* and *red curves* represent hypothetical scenarios for changes in mesor, phase, or amplitude, which is described in each plot. Representative scenarios of possible combination in rhythmic parameters that can contribute to the lack of consistent DEGs identified in different studies.

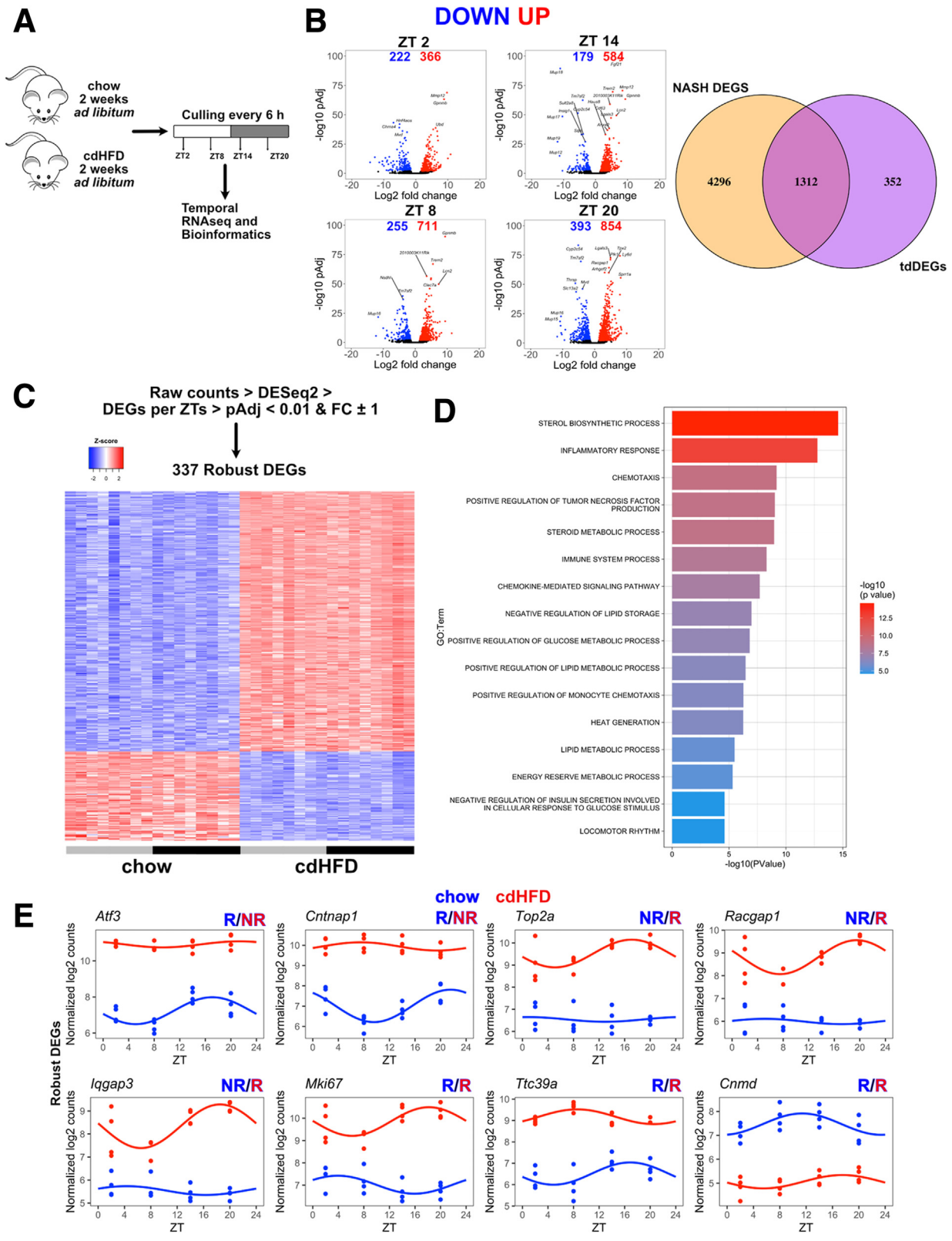

Figure 3. cdHFD results in a marked liver DEG pattern comparable with HFFC diet. (*A*) Experimental design is represented. (*B*) DEG analysis was performed for each time point (ZT) and is shown in individual volcano plots. Totals of genes down-regulated and up-regulated are shown in each graph. Genes identified in at least 1 ZT were merged into a single list and classified as tdDEGs. Venn diagram shows how many genes are exclusive and shared between the NASH DEGs and tdDEGs. (*C*) Robust DEGs were identified as being differentially expressed across all ZTs and are represented as a heatmap. (*D*) GSEA of robust DEGs. (*E*) Diurnal profile of robust DEGs that show changes in mesor, amplitude, and/or phase. n = 4 for each ZT. FC, fold change; NR, no rhythmicity; pAdj, adjusted *P* value; R, rhythmicity.

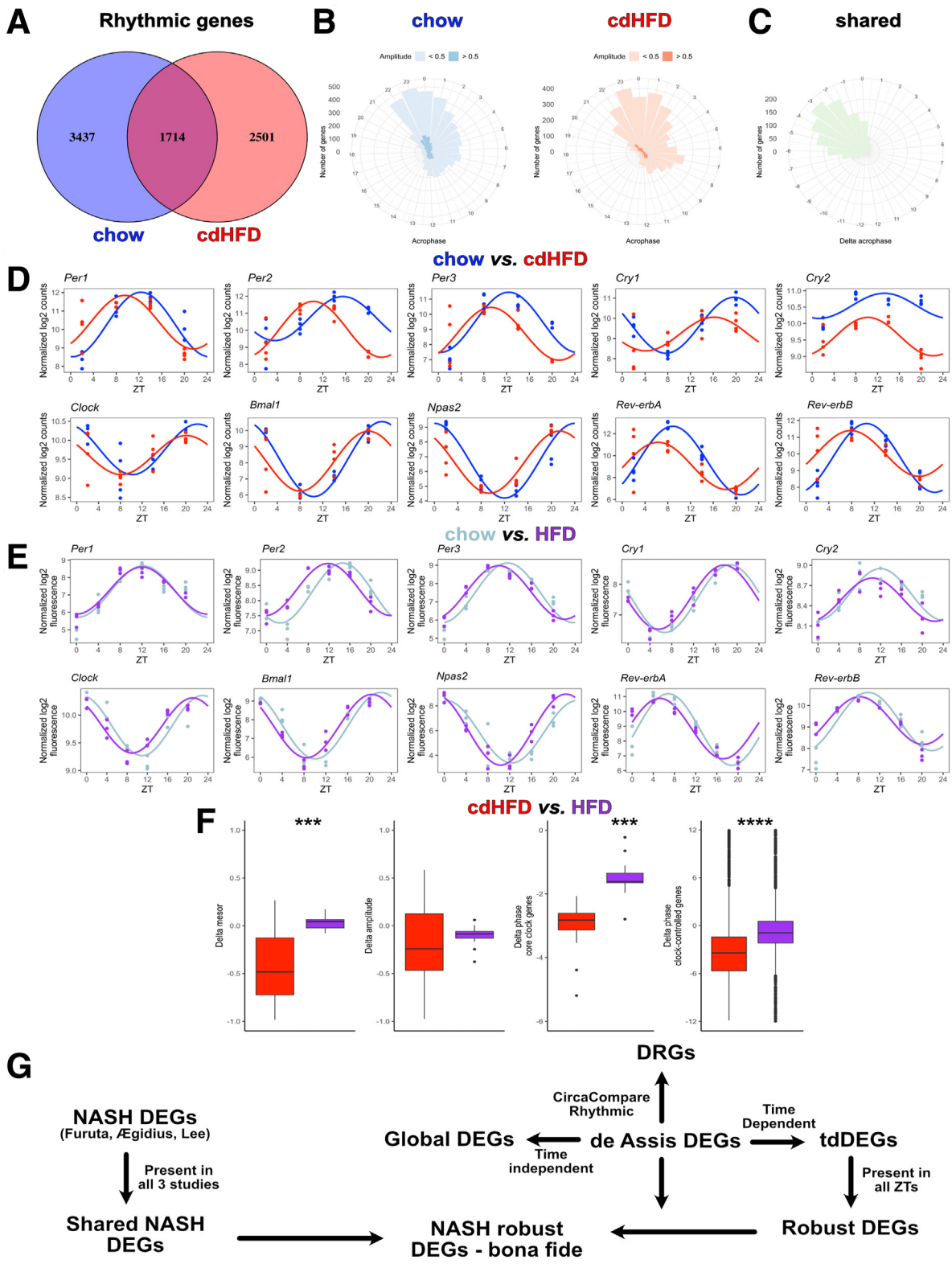

Figure 4. cdHFD results in a marked phase advance in the liver, which is stronger compared with regular HFD. (*A*) Venn diagram shows the number of rhythmic genes for each group. Rhythmicity was performed using CircaN, JTK cycle, Metacycle, and DyrR ($P < .01$). (*B* and *C*) Rose plots represent the acrophase of chow, cdHFD, and shared rhythmic genes. (*D* and *E*) Diurnal profile of chow and cdHFD livers and reanalysis of Eckel-Mahan et al[10] using our bioinformatic pipeline. (*F*) Rhythm parameter evaluation between cdHFD and HFD models. For core clock gene evaluation, a paired Mann–Whitney test was used. For chow and cdHFD, n = 4 for each time point (ZT). (*G*) Flow chart of the different classes of DEGs and DRGs used in this study. For chow and HFD, n = 3 for each ZT. ***$P < .001$, ****$P < .0001$.

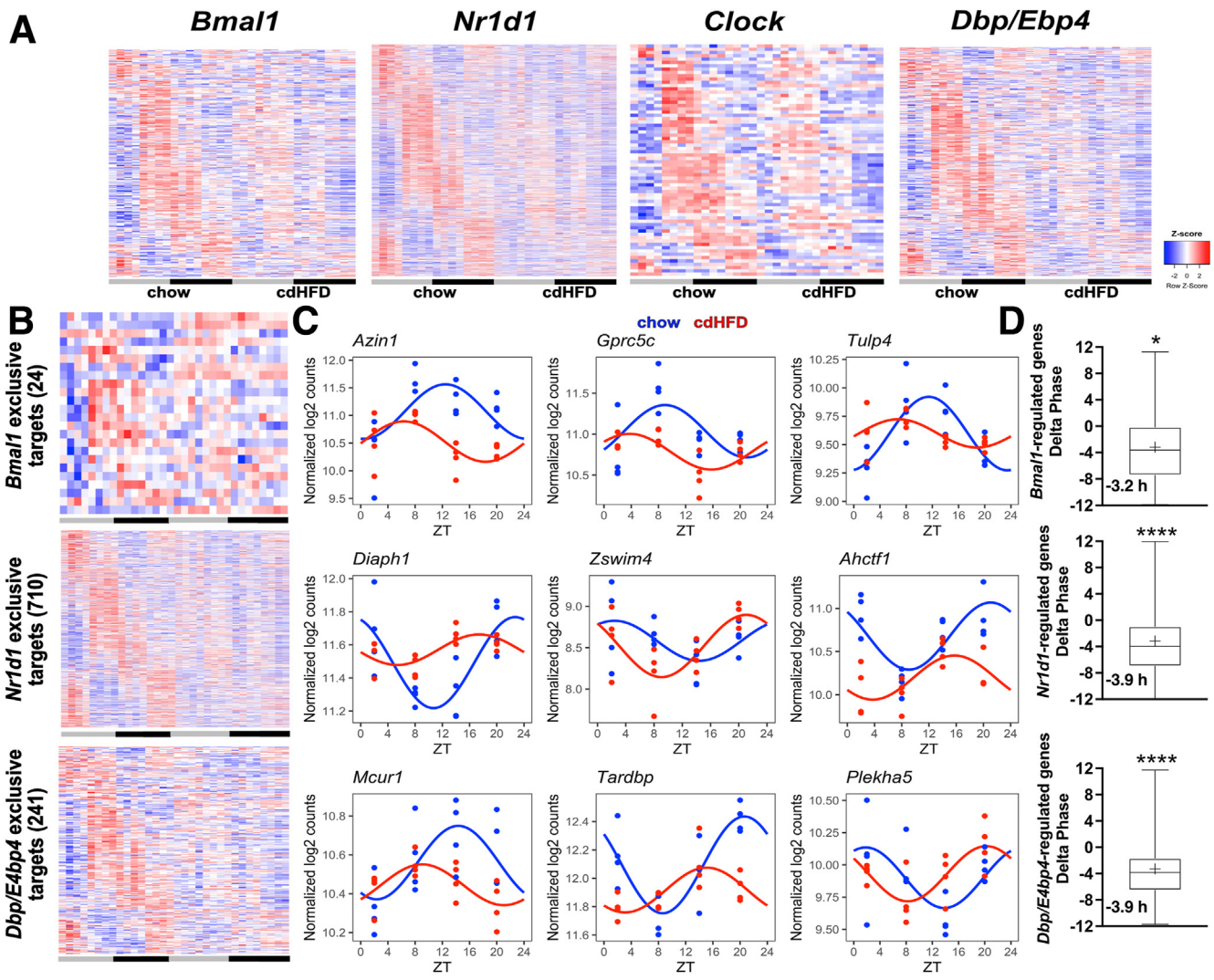

Figure 5. Transcriptional targets of clock transcription factors show a marked phase advance. (*A*) Putative targets of core clock proteins were extracted from Chipseq Atlas (except *Dbp/E4bp4*, see the Materials and Methods section) and filtered for rhythmicity according to CircaCompare. Heatmaps of each transcription factor are plotted. (*B*) Exclusive targets for each transcriptional factor were filtered and are shown in heatmaps. (*C*) Representative genes with marked phase advance are shown. (*D*) Overall phase distribution of the exclusive targets according to CircaCompare. For chow and cdHFD, n = 4 for each ZT. *$P < .05$, ****$P < .0001$ against zero.

circadian rhythm parameters in NASH compared with control livers. Most rhythmic genes were altered in mesor (n = 5062), with similar numbers for an increase or decrease. A total of 1292 genes showed amplitude changes, and most of them (90%) were dampened in NASH. A total of 1317 genes showed significant alterations in phase, of which 90% were phase advanced, in line with our previous observations (Figures 6*A* and *B* and 4*C*, Supplementary Table 5). GSEA of genes with rhythm alterations mainly yielded processes associated with cell damage repair (eg, Gene Ontology categories of cell-cycle progression and DNA repair) and processes associated with lipid metabolism (eg, lipid and fatty acid metabolism), among others (Figure 6*C*, Supplementary Table 5). A marked reduction in mesor and amplitude combined with phase advances was seen for key genes involved in lipid metabolism such as *Lipc*, *Dgat2*, *Acaca*, *Fasn*, *Crot*, *Elovl1/5/6*, and *Cpt1a* (Figure 6*D*, Supplementary Table 5). In line with this, NASH led to loss of rhythmicity (amplitude reduction) in liver triglyceride levels in addition to a marked 11-fold overall up-regulation (Figure 6*D*).

Interestingly, GSEA also detected protein ubiquitination as a NASH regulated pathway with alterations in mesor, amplitude, and phase. Ubiquitination of circadian clock proteins is a major regulator of clock period and phase.[31] In NASH, genes associated with protein ubiquitination displayed reductions in amplitude and/or mesor. For others, marked phase advances were observed (*Ube2h*, *Ube4b*, *Ube2q1*, *Ube2q2*, and *Ube2u*) (Figure 6*E*, Supplementary Table 5). These data indicate a time-dependent regulation of protein ubiquitination in the healthy liver, which is

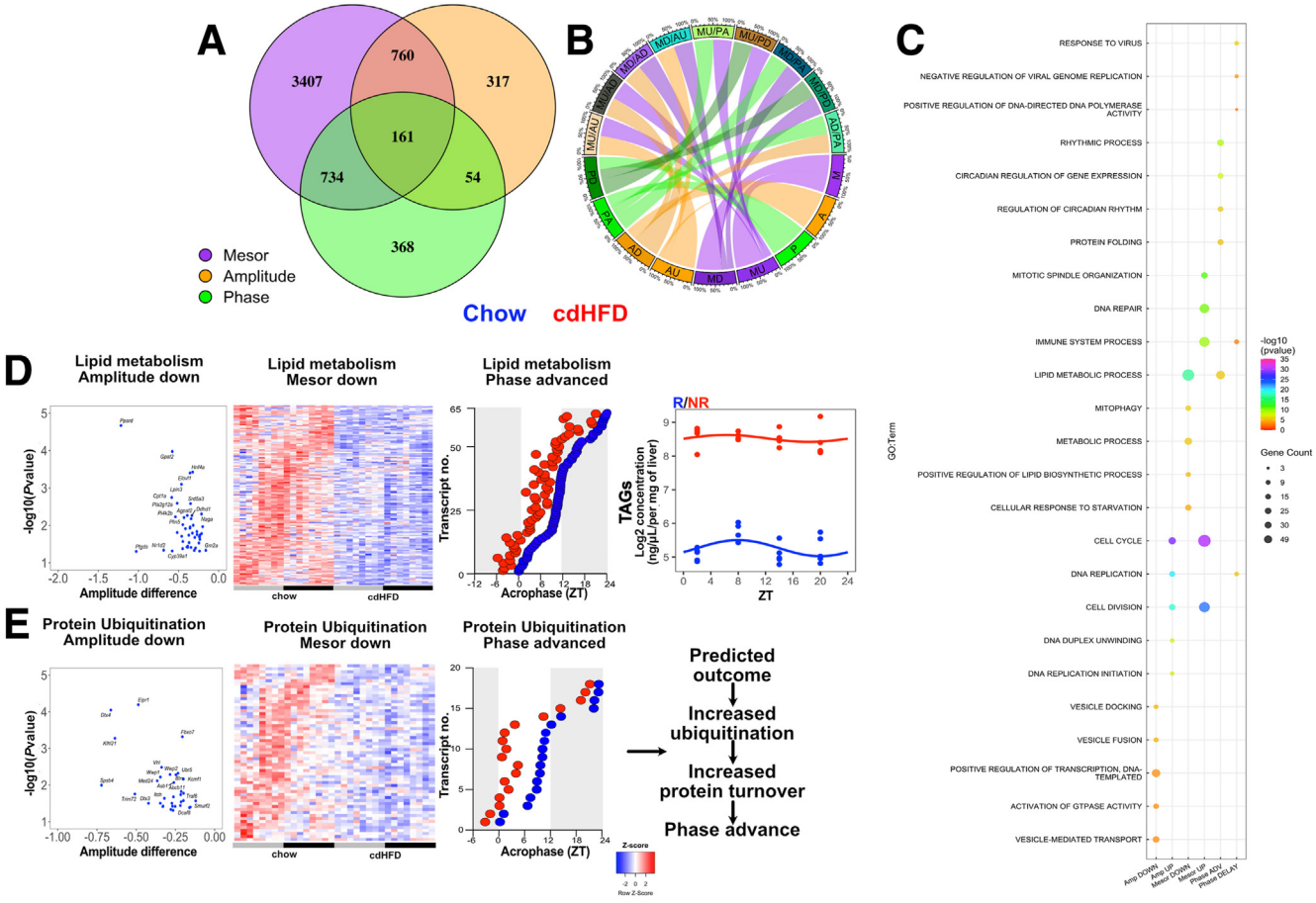

Figure 6. cdHFD leads to marked diurnal transcriptome rewiring with several metabolic biological processes affected in mesor, amplitude (Amp), or phase. (*A*) Venn diagram shows the changes in rhythm parameters detected by the CircaCompare method. (*B*) Chord plot represents the combination of rhythmic parameter alterations identified by CircaCompare. (*C*) The top 5 enriched biological processes are represented by each rhythmic parameter. (*D* and *E*) Genes related to lipid metabolism and protein ubiquitination processes are shown in heatmaps for changes in mesor. Volcano and dot plots show the amplitude and phase change for each gene that participated in a biological process, respectively. Phase was estimated according to CircaCompare. When phase was higher than 18 in the cdHFD group, phase value was subtracted from 24 and plotted to emphasize phase alteration. Liver levels of triglycerides (TAGs) are shown in $\log_2$ values. Presence and absence for rhythmicity is shown as R or NR, respectively. For RNAseq data, n = 4 for each time point (ZT). For TAG data, n = 4–5 per ZT. A, amplitude; AD, amplitude down; ADV, advance; AU, amplitude up; GO, Gene Ontology; M, mesor; MD, mesor down; MU, mesor up; NR, no rhythmicity; P, phase; PA, phase advance; PD, phase delay; R, rhythmicity.

altered by NASH. They also suggest a potential direct mechanism for NASH effects on liver clock regulation.

In summary, our comparative rhythm analysis revealed distinct alterations in biological processes associated with liver steatosis. NASH-related changes in ubiquitination transcript rhythms may contribute to the phase advance effect observed for clock and clock-controlled gene expression. Further experiments are necessary to validate this premise.

Temporal Control of Tissue Sampling Augments DEG Detection

Finally, we compared the power of temporal profiling against traditional 1-time point approaches without temporal control. From the previously identified NASH DEGs (n = 5608) detected by at least 1 of 3 studies (Figure 1), CircaCompare analysis confirmed 1875 genes with alterations in at least 1 rhythm parameter (Figure 7*A*). Of these, 1746, 356, and 361 genes showed changes in mesor, amplitude, or phase, respectively (Supplementary Table 6). In addition, our profiling approach detected 4157 DEGs with alterations in 1 or more rhythm parameters (CircaCompare; n = 3926) or overall expression (global DEGs; n = 231). A total of 568 (83%) of the DEGs consistently detected by all 3 previous studies also were detected as altered by this approach. Some examples for NASH-induced changes in expression profiles are depicted for alterations in mesor (Figure 7*B*, upper row), amplitude (Figure 7*B*, middle row), and phase (Figure 7*B*, lower row) (see Supplementary Tables 5 and 6 for a full list). Overall, this combined approach outmatched traditional DEG detection for rhythmic parameter changes by a factor of 3.

To estimate the gain in DEG detection power achieved by controlling for time in transcriptome analyses, we simulated 1-time point random-time sampling and tdDEGs from chow

and cdHFD data sets and compared these against circadian profiling on a reduced sampling (n = 3 per time point; differentially rhythmic genes [DRGs]). On average, a higher DEG detection rate of 20% was obtained when sampling time was controlled (Figure 7*C*). Of note, random sampling did not impact robust DEG detection (from the cdHFD data set) because on average 94% of robust DEGs were identified independent of sampling time. Combined circadian profiling, however, resulted in a 7-fold increase in DEGs, but coming at the cost of a 3-fold increase in sample sizes compared with 1-time point sampling (Figure 7*C*, Supplementary Table 6). GSEA analyses of the different DEG classes showed that accounting for time increased the detection of exclusive (91 of 221) biological processes compared with global and tdDEGs by 40%. As expected, processes such as circadian rhythms, fatty acid, glycogen, carbohydrates, cholesterol metabolism, and insulin signaling regulation were markedly presented in DRGs (Supplementary Table 6).

Discussion

Our findings corroborate previous NASH studies as the identified NASH gene signature is suggestive of increased DNA damage and repair,[32] disrupted cell-cycle progression, tissue repair, and apoptosis,[33] and immune system activation[34,35]. Several genes associated with these processes showed increased amplitudes in their circadian expression rhythms, which suggests a stronger level of temporal control. Processes such as lipid and glucose metabolism showed decreased gene expression (mesor down) in NASH livers, thus suggesting an overall activity reduction of energy metabolic pathways. Genes associated with lipid, glucose, and glycogen metabolism also showed reduced amplitude in their daily rhythms or phase advances. A similar phase advance in core clock genes was found, suggesting a clock-mediated mechanism. This idea was supported further by phase shifts in bona fide direct clock target genes.

One limitation of our study lies on the low circadian resolution (every 6 hours), which can increase the number of false positives. Upon estimating rhythmicity, we adopted a rather strict uniform *P* value cut-off level across the different methods to assess rhythmicity. Other parameters such as amplitude and/or cosine curve fits were not considered, which also can increase false-positive detection. One might argue that such phase effects are associated with the high steatosis environment induced by cdHFD. Upon evaluating a previous study that used a HFD,[10] we indeed identified a phase advance in gene expression rhythms, albeit to a much lesser extent (Figure 4). Therefore, the presence of a high lipid environment indeed contributes to the phase advancement, but such effect is enhanced further by pathologic events in the NASH liver. Proper molecular clock functioning is dependent on cycles of protein synthesis and degradation. The first clock mutant (tau) discovered[36] had a shorter locomotor activity period. A subsequent study identified casein kinase 1ε as responsible for such an event because of its capacity to phosphorylate PERIOD (PER). Increased PER degradation as a consequence of defective casein kinase 1ε phosphorylation resulted in a shorter circadian period.[37,38] Protein degradation is mediated primarily via ubiquitination and targeting to proteasomes. Several clock proteins are subject to ubiquitination, which provides a mechanism for period fine-tuning and phase adjustment.[31] We suggest that disrupted ubiquitination signaling may result in increased clock protein degradation, which, in turn, can phase-advance the core clock (Figure 6). Interestingly, increased ubiquitination levels have been detected previously in human NASH and were suggested as a marker as well as a driver of NASH pathology.[39,40]

The observed phase advance in liver glucose metabolism transcripts may have systemic consequences and trigger a compensatory response to normalize serum glucose levels. Similarly, a phase advance in liver lipid metabolism transcripts may shift systemic energy substrate bioavailability to an earlier time. Previous findings showing that HFD-fed mice display increased food consumption during the light (rest) phase[41] corroborated our findings, despite the differences in diet composition. A systemic phase advance in liver transcript rhythms may result in misalignment between geophysical (external) and internal time, affecting metabolic efficiency. In a second potential scenario such phase advance would be restricted to the liver or the liver and a few metabolic organs. Such internal circadian misalignment was shown for HFD conditions in which shifts mostly were restricted to insulin-sensitive organs.[42] Similarly, NASH-induced transcriptome changes could contribute to tissue decoupling, further propagating metabolic pathologies and NASH progression.[18] Vice versa, addressing such phase shifts by external zeitgebers could slow down or prevent NASH, and such applications warrant further investigation.

From a medical standpoint, any changes in rhythm parameters are relevant for the optimization of NASH therapies. Alterations in expression mesor of a relevant gene indicate that the goal of treatment is to modify overall levels of expression or activity, and this goal may be achieved independent of treatment time. This scenario changes once a gene shows an amplitude or a phase effect. Now, the time of treatment may critically determine the therapeutic outcome. NASH-induced phase effects may call for a reduction in activity at one time and an increase at another (Figure 1*D*). To avoid such complexity, it may be advisable to attempt to stabilize the circadian clock itself and in this way indirectly rectify clock-controlled gene (CCG) output instead of targeting specific genes/processes.[43] Considering the changes found in our study, we suggest that clock strengthening either by a pharmacologic approach[44] and/or time restricted feeding[45] may benefit NASH treatment. Chronomodulated pharmacologic approaches have been suggested in NASH treatment.[46]

Although time is an important regulatory element for health,[3] the control for or evaluation of (day-) time as a variable factor often is neglected in many research fields.[6] We hypothesized that a lack of control for sampling time augments inconsistencies in results between different NASH studies that used a similar NASH-inducing model. Upon selecting 3 independent but similar studies,[22–24] only a

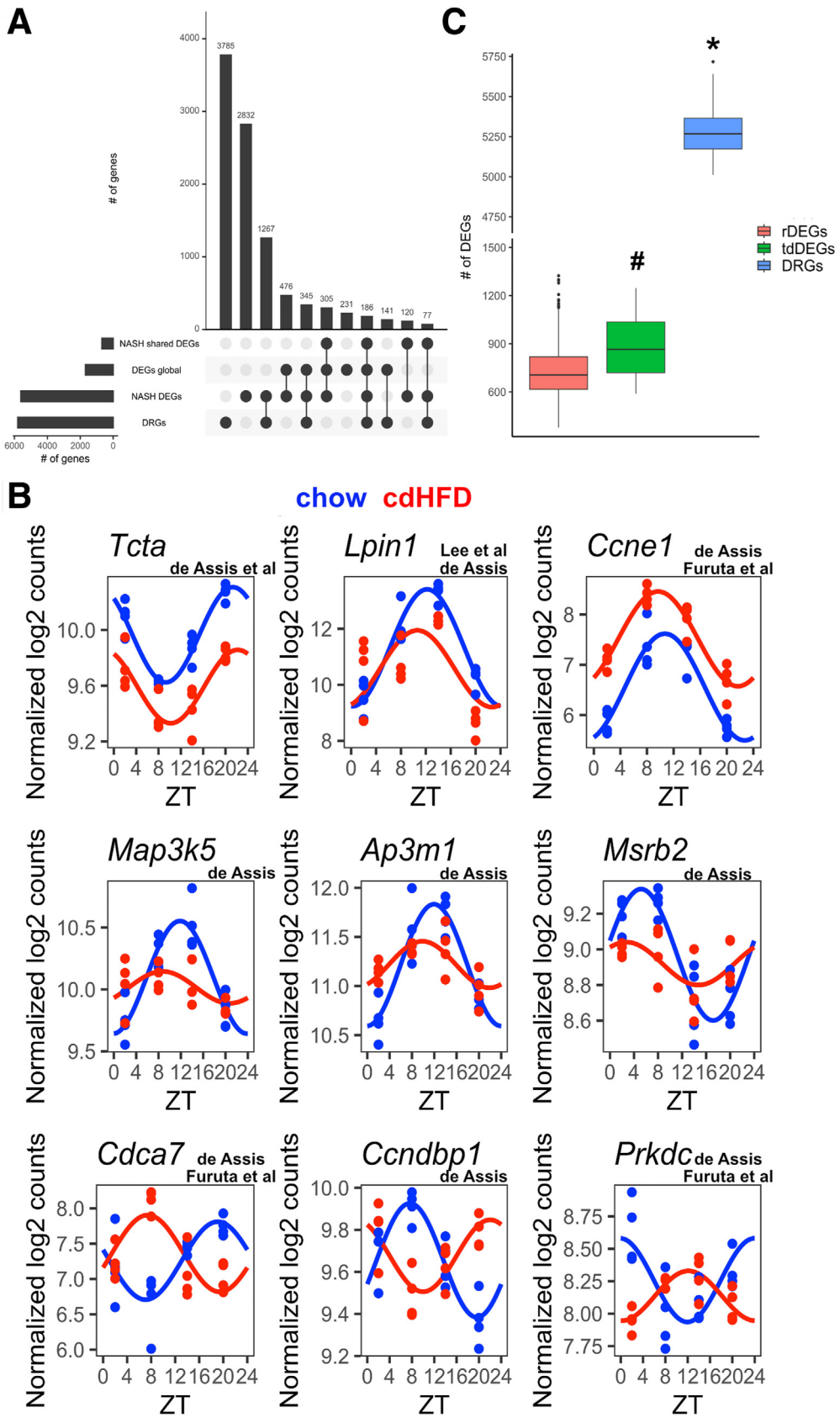

Figure 7. Accounting for sampling time results in increased DEG detection and higher reproducibility of NASH models. (*A*) Venn diagram represents the number of DEGs identified in at least 1 published study (DEGs published), DEGs identified in all 3 studies (DEGs published robust), DEGs identified in our data set disregarding sampling time (DEGs global), and DRGs. (*B*) Representative plots for DEGs that show mesor (*upper row*), amplitude (*middle row*), or phase effect (*lower row*). On top of each gene is shown the study in which such gene was identified. (*C*) Comparison among DEGs generated by random sampling (rDEGs), tdDEGs, and time-controlled sampling followed by DRGs. *Statistical difference ($P < .001$) against rDEGs and tdDEGs. #Difference against rDEGs ($P = .029$). For chow and cdHFD, n = 4 for each time point (ZT).

small fraction of DEGs were identified consistently (12%), and many DEGs detected by either one of these studies showed rhythmic regulation of expression across the day.[11] It has been shown previously that 3 weeks of cdHFD does not lead to fibrosis.[28] However, longer exposure to NASH-inducing diets such as HFFC is known to lead to fibrosis.[22–24] One could consider our experimental model and the studies from the literature (NASH DEGs) as early and late-type NASH, respectively. Therefore, this can be considered an important source of variation that might explain the incomplete overlap between the studies.

To estimate the impact of not having temporal control on sampling, we determined DEG yields using randomized sampling under time-controlled and time-ignorant conditions and compared these against circadian profiling. We confirmed that lack of proper temporal control hampers the detection of DEGs (Figure 7). Moreover, by performing circadian rhythm analyses, we identified approximately 7-fold more DEGs. Our findings clearly show the consequences for not accounting for time, which can result in increased false positives and lack of consistency between similar NASH studies.

The marked NASH effects observed on the circadian phase of liver transcripts warrant particular attention. Such phase changes, either delays or advances, could be interpreted mistakenly as up-regulation or down-regulation, depending on the time point of assessment. This, in turn, may affect therapy targets. However, with a circadian perspective, more informed decisions on therapeutic strategies could be made. Clearly, considering circadian rhythms in NASH will provide a more comprehensive understanding of the molecular underpinnings of this disease with high therapeutic potential beyond the development of novel compounds.

Materials and Methods

Mouse Model and Experimental Conditions

Two- to 3-month-old male and female wild-type (C57BL/6J) mice were group-housed under 12-hour/12-hour light/dark conditions (LD, 200–400 lux) at 22°C ± 2°C with food and water provided ad libitum. After 1 week of acclimatization under NC (5% fat, 1314; Altromin) NASH was induced by switching to a cdHFD (9% protein, 60% fat, 2% cholesterol, and 31% carbohydrate, 0.17% methionine, E15673-94; Ssniff) for 2 weeks. NASH and control mice (on NC) were killed by cervical dislocation at 6-hour intervals and tissues were flash-frozen in N_2 and stored at -80°C. Animal experiments were ethically approved by the Animal Health and Care Committee of the Government of Schleswig–Holstein and were in line with international guidelines for the ethical use of animals. Even numbers of males and females were used for all conditions except for cdHFD at time point (ZT) 14, with 1 female and 3 males.

RNAseq

Total RNA was extracted from livers using TRIzol reagent (Thermofisher) and spin-columns (Zymo Research) according to the manufacturer's instructions. Trueseq RNAseq comprising 40 million reads per sample (12 GB) was performed at Novogene. Samples underwent quality control and only those with a RNA integrity number higher than 6.5 were used. Messenger RNA was purified from total RNA using poly-T oligo-attached magnetic beads. After fragmentation, the first-strand complementary DNA was synthesized using random hexamer primers, followed by the second-strand complementary DNA synthesis using deoxythymidine triphosphate (dTTP) for nondirectional library. The library was checked with Qubit and real-time polymerase chain reaction for quantification and a bioanalyzer for size distribution detection. The clustering of the index-coded samples was performed according to the manufacturer's instructions. After cluster generation, the library preparations were sequenced on an Illumina platform and paired-end reads were generated. Raw data (raw reads) of fastq format were first processed through in-house perl scripts. In this step, clean data (clean reads) were obtained by removing reads containing adapter, reads containing ploy-N, and low-quality reads from raw data. At the same time, quality scores (Q20, Q30) and guanine-cytosine content (GC) content for the clean data were calculated.

Reference genome (GRCm38/mm10) and gene model annotation files were downloaded from genome website browsers NCBI/UCSC/ENSEMBL directly. Paired-end clean reads were mapped to the reference genome using HISAT2 software. HISAT2 uses a large set of small graph FM index (GFM) indexes that collectively cover the whole genome. These small indexes (called *local indexes*), combined with several alignment strategies, enable rapid and accurate alignment of sequencing reads. All of the downstream analyses were based on the clean data with high quality. FeatureCounts was used to count the read numbers mapped to each gene. Genes containing a sum of reads among 2 groups lower than 100 were excluded from analysis. The remaining genes were $\log_2$ transformed in DESeq2 using the *vsd* function (blind = FALSE). A total of 18,980 transcripts were considered for subsequent analyses.

DEG Analysis

To identify DEGs independent of sampling time, we used DESeq2[25] with an adjusted P value of .01 and a $\log_2$ fold-change of ±1 as cut-off values for pooling samples from all time points (ZTs). For time point–specific DEGs, DESeq2 was performed separately for each ZT. Data from 3 independent mouse NASH RNAseq studies (Lee et al,[22] GSE162249; Furuta et al,[23] GSE164084; and Ægidius et al,[24] GSE195483) were downloaded from GEO (https://www.ncbi.nlm.nih.gov/geo) and processed as described earlier. Of note, genetic background of mice and diet interventions (HFFC: 40% fat, 20% fructose, and 2% cholesterol for 24–36 weeks) were largely comparable between the 3 studies. They differed, however, in light conditions (LD 12:12 for Ægidius et al,[24] Furuta et al,[23] and our study; LD 14:10 for Lee et al[22]).

Rhythm Analyses

To identify diurnal (24-hour) oscillations in gene expression, we combined 4 independent algorithms: CircaN,[47] Jonckheere-Terpstra-Kendall (JTK) cycle,[48]

Metacycle,[49] and DryR.[50] CircaCompare was used to compare rhythmic parameters between groups.[51] For mesor and amplitude comparison, CircaCompare was allowed to fit a sine curve irrespective of meeting rhythmicity thresholds. Phase comparison was performed only in robustly rhythmic genes as described.[26] CircaN, JTK cycle, and Metacycle algorithms were run in a CircaN algorithm using the default parameters. An exact period of 24 hours was used. The significance of rhythmicity was set as $P < .01$ for each method. Rhythmic genes were combined into a single list for each group, followed by rhythm parameters comparison using CircaCompare algorithm.[51]

Data sets from Zhang et al[11] and Eckel-Mahan et al[10] were extracted; $\log_2$ (value +1) normalized; and CircaN, JTK cycle, and Metacycle were used to evaluate rhythmicity. The DryR method was not included in this analysis owing to high temporal resolution and because adding DryR only led to a marginal increase (approximately 10%) in novel gene rhythmicity detection in our RNAseq analysis (6-hour profile). For the Zhang et al[11] study, each time point consisted of 1 sample every 2 hours. For the Eckel-Mahan et al[10] study, each time point consisted of 3 samples every 4 hours. For all comparisons in CircaCompare, a *P* value of .05 was used. For heatmap and rose plots, phase estimation was extracted from CircaCompare. Rhythmic gene visualization was made using CircaCompare algorithm.

Reanalysis of Chipseq Analyses

Target genes of transcriptional factors were obtained using the Chipseq Atlas.[30] Putative targets genes were selected by selecting genes up to 10,000 bases from the transcription start sites of mice (*Mus musculus*, mm9 or mm10). Targets genes were filtered for redundancy and only those with an average score greater than 250 were selected for rhythmicity evaluation using CircaCompare data set. For DBP/E4bp4, data were extracted from the original study.[52] All putative targets were analyzed against our rhythmicity analysis data set.

GSEA

Enrichment analyses were performed using Gene Ontology annotations for Biological Processes with DAVID 6.8 software[53] and cut-off values of 3 genes per process and a *P* value less than .05. REVIGO (reduction of 0.5 and default conditions) was used to reduce redundant calls in GSEA.[54]

Random-Sampling DEG Evaluation

To estimate the effect of time-controlled sampling on the power of DEG detection, we generated 1000 data sets without time control by randomly picking combinations of 4 samples from the diurnal profile data. DEG evaluation was performed using DESeq2, as described. In addition, a total of 100 temporal profile data sets for NC and cdHFD mice with 4 sampling times and 3 samples per ZT were randomly generated. Previously identified rhythmic genes (using the whole data set) were kept constant for each generated data set and used for CircaCompare analysis. Genes with alteration in rhythmic parameters were merged and classified as DRGs. Comparison between different classes of DEGs was made by using permutation analysis (lmPerm, permutation "Exact"). A *P* value less than .05 was considered significant.

Histologic Evaluation

For H&E staining, livers were collected, washed with phosphate-buffered saline, and fixed in paraformaldehyde (4%; Electron Microscopy Sciences) for 48 hours, followed by dehydration with increasing concentrations of ethanol. Livers were embedded in paraffin and cut into 5- to 10-μm slices. After dewaxing and dehydration, slices were stained with H&E for light microscope examination. For Oil Red O(ORO) staining, livers were collected, washed with phosphate-buffered saline, and snap-frozen in liquid nitrogen. Liver tissue was embedded in optimal cutting temperature (OCT) compound, and 10-μm sections were made with a cryostat. ORO staining was performed according to an established protocol.[55]

Triglyceride and Cholesterol Evaluation

Tissue triglyceride and cholesterol were processed according to the manufacturer's instructions (MAK266; Sigma-Aldrich; STA 384; Cell Biolabs).

Liver Damage Marker Evaluation

Plasma from NC and cdHFD mice was used to quantify aspartate aminotransferase activity using commercial kits (MAK055; Sigma-Aldrich). NC and cdHFD were diluted 5 and 10 times, respectively.

Data Handling and Statistical Analysis

Samples were excluded only upon technical failure. Analyses were performed in Prism 9.4 (GraphPad) with a cut-off *P* value of .05. Two-group comparisons were performed by Student *t* test with Welch correction, or Mann–Whitney test for parametric or nonparametric samples, respectively. Normality evaluation was performed using the Shapiro–Wilk test. All transcriptome analyses were conducted using R

Table 1.R Packages Used in the Bioinformatic Analysis

Name	Version	Use
Eulerr	6.1.1	Venn diagram
VennDiagram	1.7.1	Venn diagram
CircaCompare	0.1.1	Graph and rhythm comparisons
CircaN	2.0.0	Rhythm analysis
DyrR	1.0.0	Rhythm analysis
DESeq2	1.32.0	Differentially expressed genes
Gplot	3.1.3	Heatmap generation
Gplot2	3.3.5	Graph generation
GraphPad	9.1	Graph generation
Circlize	0.4.14	Chord plot
lmPerm	2.1.1.	Permutation analysis
ggbreak	0.1.0	Graph generation
UpSetR	1.4.0	Graph generation

4.2.1 (R Foundation for Statistical Computing) or in Prism 9.4 (GraphPad). The R packages used are described in Table 1.

References

1. Gerhart-Hines Z, Lazar MA. Circadian metabolism in the light of evolution. Endocr Rev 2015;36:289–304.
2. West AC, Bechtold DA. The cost of circadian desynchrony: evidence, insights and open questions. Bioessays 2015;37:777–788.
3. de Assis LVM, Oster H. The circadian clock and metabolic homeostasis: entangled networks. Cell Mol Life Sci 2021;78:4563–4587.
4. Kovac J, Husse J, Oster H. A time to fast, a time to feast: the crosstalk between metabolism and the circadian clock. Mol Cells 2009;28:75–80.
5. Brown SA. Circadian metabolism: from mechanisms to metabolomics and medicine. Trends Endocrinol Metab 2016;27:415–426.
6. Nelson RJ, Bumgarner JR, Liu JA, et al. Time of day as a critical variable in biology. BMC Biol 2022;20:142.
7. Hurni C, Weger BD, Gobet C, Naef F. Comprehensive analysis of the circadian nuclear and cytoplasmic transcriptome in mouse liver. PLoS Genet 2022;18:e1009903.
8. Mure LS, Le HD, Benegiamo G, et al. Diurnal transcriptome atlas of a primate across major neural and peripheral tissues. Science 2018;359:eaao0318.
9. Robles MS, Cox J, Mann M. In-vivo quantitative proteomics reveals a key contribution of post-transcriptional mechanisms to the circadian regulation of liver metabolism. PLoS Genet 2014;10:e1004047.
10. Eckel-Mahan KL, Patel VR, de Mateo S, et al. Reprogramming of the circadian clock by nutritional challenge. Cell 2013;155:1464–1478.
11. Zhang R, Lahens NF, Ballance HI, et al. A circadian gene expression atlas in mammals: implications for biology and medicine. Proc Natl Acad Sci U S A 2014;111:16219–16224.
12. Riazi K, Azhari H, Charette JH, et al. The prevalence and incidence of NAFLD worldwide: a systematic review and meta-analysis. Lancet Gastroenterol Hepatol 2022;7:851–861.
13. Eslam M, Sanyal AJ, George J. MAFLD: a consensus-driven proposed nomenclature for metabolic associated fatty liver disease. Gastroenterology 2020;158:1999–2014.e1.
14. Haas JT, Francque S, Staels B. Pathophysiology and mechanisms of nonalcoholic fatty liver disease. Annu Rev Physiol 2016;78:181–205.
15. Friedman SL, Neuschwander-Tetri BA, Rinella M, Sanyal AJ. Mechanisms of NAFLD development and therapeutic strategies. Nat Med 2018;24:908–922.
16. Rijo-Ferreira F, Takahashi JS. Genomics of circadian rhythms in health and disease. Genome Med 2019;11:82.
17. Stenvers DJ, Scheer FAJL, Schrauwen P, et al. Circadian clocks and insulin resistance. Nat Rev Endocrinol 2019;15:75–89.
18. de Assis LVM, Demir M, Oster H. The role of the circadian clock in the development, progression, and treatment of non-alcoholic fatty liver disease. Acta Physiol 2023;237:e13915.
19. Kettner NM, Voicu H, Finegold MJ, et al. Circadian homeostasis of liver metabolism suppresses hepatocarcinogenesis. Cancer Cell 2016;30:909–924.
20. Suppli MP, Rigbolt KTG, Veidal SS, et al. Hepatic transcriptome signatures in patients with varying degrees of nonalcoholic fatty liver disease compared with healthy normal-weight individuals. Am J Physiol Gastrointest Liver Physiol 2019;316:G462–G472.
21. Xiong X, Wang Q, Wang S, et al. Mapping the molecular signatures of diet-induced NASH and its regulation by the hepatokine Tsukushi. Mol Metab 2019;20:128–137.
22. Lee SM, Pusec CM, Norris GH, et al. Hepatocyte-specific loss of PPARγ protects mice from NASH and increases the therapeutic effects of rosiglitazone in the liver. Cell Mol Gastroenterol Hepatol 2021;11:1291–1311.
23. Furuta K, Guo Q, Pavelko KD, et al. Lipid-induced endothelial vascular cell adhesion molecule 1 promotes nonalcoholic steatohepatitis pathogenesis. J Clin Invest 2021;131:e143690.
24. Ægidius HM, Veidal SS, Feigh M, et al. Multi-omics characterization of a diet-induced obese model of non-alcoholic steatohepatitis. Sci Rep 2020;10:1148.
25. Love MI, Huber W, Anders S. Moderated estimation of fold change and dispersion for RNA-seq data with DESeq2. Genome Biol 2014;15:550.
26. de Assis LVM, Harder L, Lacerda JT, et al. Rewiring of liver diurnal transcriptome rhythms by triiodothyronine (T3) fmentation. Elife 2022;11:e79405.
27. Takahashi Y, Fukusato T. Chapter 13-animal models of liver diseases. In: Conn PM, ed. Animal models for the study of human disease. 2nd ed. Academic Press, 2017:313–339.
28. Matsumoto M, Hada N, Sakamaki Y, et al. An improved mouse model that rapidly develops fibrosis in non-alcoholic steatohepatitis. Int J Exp Pathol 2013;94:93–103.
29. Pafili K, Roden M. Nonalcoholic fatty liver disease (NAFLD) from pathogenesis to treatment concepts in humans. Mol Metab 2021;50:101122.
30. Oki S, Ohta T, Shioi G, et al. ChIP-Atlas: a data-mining suite powered by full integration of public ChIP-seq data. EMBO Rep 2018;19:e46255.
31. Srikanta SB, Cermakian N. To Ub or not to Ub: regulation of circadian clocks by ubiquitination and deubiquitination. J Neurochem 2021;157:11–30.
32. Daugherity EK, Balmus G, Al Saei A, et al. The DNA damage checkpoint protein ATM promotes hepatocellular apoptosis and fibrosis in a mouse model of non-alcoholic fatty liver disease. Cell Cycle 2012;11:1918–1928.
33. Caldez MJ, Bjorklund M, Kaldis P. Cell cycle regulation in NAFLD: when imbalanced metabolism limits cell division. Hepatol Int 2020;14:463–474.
34. Sutti S, Albano E. Adaptive immunity: an emerging player in the progression of NAFLD. Nat Rev Gastroenterol Hepatol 2020;17:81–92.
35. Ganz M, Szabo G. Immune and inflammatory pathways in NASH. Hepatol Int 2013;7(Suppl 2):771–781.
36. Ralph MR, Menaker M. A mutation of the circadian system in golden hamsters. Science 1988;241:1225–1227.

37. Loudon A, Meng Q-J, Maywood ES, et al. The biology of the circadian Ck1ε tau mutation in mice and Syrian hamsters: a tale of two species. Cold Spring Harb Symp Quant Biol 2007;72:261–271.
38. Lowrey PL, Shimomura K, Antoch MP, et al. Positional syntenic cloning and functional characterization of the mammalian circadian mutation tau. Science 2000; 288:483–492.
39. Park J-S, Ma H, Roh Y-S. Ubiquitin pathways regulate the pathogenesis of chronic liver disease. Biochem Pharmacol 2021;193:114764.
40. Xin S, Yu Y. Ubiquitin-specific peptidase 10 ameliorates hepatic steatosis in nonalcoholic steatohepatitis model by restoring autophagic activity. Dig Liver Dis 2022; 54:1021–1029.
41. Kohsaka A, Laposky AD, Ramsey KM, et al. High-fat diet disrupts behavioral and molecular circadian rhythms in mice. Cell Metab 2007;6:414–421.
42. Ribas-Latre A, Fekry B, Kwok C, et al. Rosiglitazone reverses high fat diet-induced changes in BMAL1 function in muscle, fat, and liver tissue in mice. Int J Obes (Lond) 2019;43:567–580.
43. Kramer A, Lange T, Spies C, et al. Foundations of circadian medicine. PLoS Biol 2022;20:e3001567.
44. Rasmussen ES, Takahashi JS, Green CB. Time to target the circadian clock for drug discovery. Trends Biochem Sci 2022;47:745–758.
45. Acosta-Rodríguez VA, Rijo-Ferreira F, Green CB, Takahashi JS. Importance of circadian timing for aging and longevity. Nat Commun 2021;12:2862.
46. Marjot T, Ray DW, Tomlinson JW. Is it time for chronopharmacology in NASH? J Hepatol 2022;76:1215–1224.
47. Rubio-Ponce A, Ballesteros I, Quintana JA, et al. Combined statistical modeling enables accurate mining of circadian transcription. NAR Genom Bioinform 2021;3:lqab031.
48. Hughes ME, Hogenesch JB, Kornacker K. JTK_CYCLE: an efficient nonparametric algorithm for detecting rhythmic components in genome-scale data sets. J Biol Rhythms 2010;25:372–380.
49. Wu G, Anafi RC, Hughes ME, et al. MetaCycle: an integrated R package to evaluate periodicity in large scale data. Bioinformatics 2016;32:3351–3353.
50. Weger BD, Gobet C, David FPA, et al. Systematic analysis of differential rhythmic liver gene expression mediated by the circadian clock and feeding rhythms. Proc Natl Acad Sci 2021;118:e2015803118.
51. Parsons R, Parsons R, Garner N, et al. CircaCompare: a method to estimate and statistically support differences in mesor, amplitude and phase, between circadian rhythms. Bioinformatics 2020;36:1208–1212.
52. Yoshitane H, Asano Y, Sagami A, et al. Functional D-box sequences reset the circadian clock and drive mRNA rhythms. Commun Biol 2019;2:300.
53. Huang DW, Sherman BT, Lempicki RA. Systematic and integrative analysis of large gene lists using DAVID bioinformatics resources. Nat Protoc 2009; 4:44–57.
54. Supek F, Bošnjak M, Škunca N, Šmuc T. REVIGO summarizes and visualizes long lists of gene ontology terms. PLoS One 2011;6:e21800.
55. Mehlem A, Hagberg CE, Muhl L, et al. Imaging of neutral lipids by oil red O for analyzing the metabolic status in health and disease. Nat Protoc 2013;8:1149–1154.

Received January 25, 2023. Accepted May 23, 2023.

Correspondence
Address correspondence to: Leonardo V. M. de Assis, PhD, Center of Brain Behavior and Metabolism, Institute of Neurobiology, University of Lübeck, Marie Curie Street, 23562 Lübeck, Germany. e-mail: leonardo.deassis@uni-luebeck.de; or Henrick Oster, PhD, Center of Brain Behavior and Metabolism, Institute of Neurobiology, University of Lübeck, Marie Curie Street, 23562 Lübeck, Germany. e-mail: henrik.oster@uni-luebeck.de.

CRediT Authorship Contributions
Leonardo VM de Assis (Conceptualization: Lead; Data curation: Lead; Formal analysis: Lead; Investigation: Lead; Writing – original draft: Lead; Writing – review & editing: Supporting)
Münevver Demir (Conceptualization: Supporting; Methodology: Supporting; Writing – review & editing: Supporting)
Henrik Oster (Conceptualization: Lead; Funding acquisition: Lead; Methodology: Supporting; Project administration: Lead; Supervision: Lead; Writing – original draft: Supporting; Writing – review & editing: Lead)

Conflicts of interest
The authors disclose no conflicts.

Funding
This work was supported by grants 353-10/1, GRK-1957, and CRC/TR 296 LOCOTACT (TP-13) from the German Research Foundation (H.O.).

Data Availability
RNAseq data are deposited in Gene Expression Omnibus under access code GSE217492.